ACS APPLIED MATERIALS & INTERFACES

Research Article

Cite This: ACS Appl. Mater. Interfaces 2018, 10, 835−844

www.acsami.org

Temperature Gradient-Induced Instability of Perovskite via Ion Transport

Xinwei Wang,[†,§] Hong Liu,*[,†,§] Feng Zhou,[†] Jeremy Dahan,[‡] Xin Wang,[†] Zhengping Li,[†] and Wenzhong Shen*[,†]

[†]Key Laboratory of Artificial Structures and Quantum Control (Ministry of Education), Institute of Physics and Astronomy, Shanghai Jiao Tong University, 800 Dong Chuan Road, Shanghai 200240, People's Republic of China

[‡]MINES Paris Tech, 60, Boulevard Saint-Michel, 75272 Paris Cedex 06, France

Supporting Information

ABSTRACT: Perovskite has been known as a promising novel material for photovoltaics and other fields because of its excellent opto-electric properties and convenient fabrication. However, its stability has been a widely known haunting factor that has severely deteriorated its application in reality. In this work, it has been discovered for the first time that perovskite can become significantly chemically unstable with the existence of a temperature gradient in the system, even at temperature far below its thermal decomposition condition. A study of the detailed mechanism has revealed that the existence of a temperature gradient could induce a mass transport process of extrinsic ionic species into the perovskite layer, which enhances its decomposition process. Moreover, this instability could be effectively suppressed with a reduced temperature gradient by simple structural modification of the device. Further experiments have proved the existence of this phenomenon in different perovskites with various mainstream substrates, indicating the universality of this phenomenon in many previous studies and future research. Hopefully, this work may bring deeper understanding of its formation mechanisms and facilitate the general development of perovskite toward its real application.

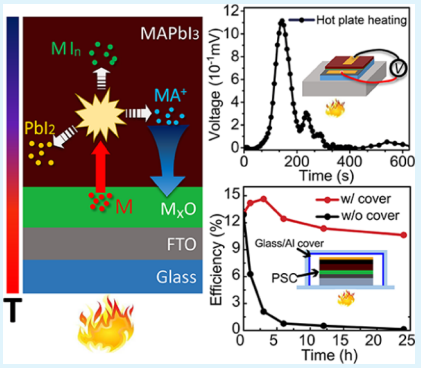

KEYWORDS: *perovskite, stability, temperature gradient, ion transport, photovoltaics.*

1. INTRODUCTION

Perovskite solar cells (PSCs) have attracted increasing attention because of their impressive high efficiency, low cost, and fabrication requirement.[1−5] The recent certified record has reached 22.1%,[6] showing potential competence even with high-performance crystalline Si solar cells. Nevertheless, the instability of perovskite has been for long time a well-known obstacle toward real applications.[7−9] It actually encompasses the phenomena of following aspects: (1) deformation or decomposition of perovskite under certain conditions (chemical and physical environments, substrate);[10] (2) drastic decrease of performance when expanding to a scale larger than 1 cm^2;[11] and (3) reproducibility issues.[12] Among these problems, the first issue is the most essential one, where many opinions have been proposed and lots of efforts have been devoted to resolve it.

Depending on the origin, the instability of perovskite can be induced by light, electricity, chemicals, and heat. According to current mainstream opinions, the photo instability of perovskite is normally weak under standard illumination.[13] The thermal instability has not been intensively discussed, as the normal fabrication is carried out under low temperature (<150 °C). It is widely accepted that thermal annealing at about 70−100 °C would be necessary for the good crystallization of perovskite and for optimization of PSCs.[14−17] The electrical instability (or the "electrical hysteresis") is known as a normal phenomenon for unmodified perovskite that the reverse and forward scanning results in different $J-V$ curves, which is reversible and has been claimed to be due to different carrier mobilities.[18,19] The chemical instability has been most intensively discussed because it can directly lead to actual decomposition of the perovskite and is irreversible in most cases.[20] This instability has significantly influenced the real application of not only perovskite itself but also some promising candidates for other parts of the cell, namely, the electrodes, the hole-transporting layer (HTL), and the electron-transporting layer (ETL). For instance, ZnO, which has 1 order higher mobility and a lower synthesis temperature than TiO_2, was regarded as a good substitutive ETL material for PSCs.[21,22] However, many researchers have demonstrated the dramatic decomposition of the $CH_3NH_3PbI_3$ perovskite film on ZnO ETL during the annealing process (heating temperature >80 °C).[23,24] Hence, most high records have been either based on modified TiO_2 or other ETL materials.

Received: November 22, 2017
Accepted: December 19, 2017
Published: December 19, 2017

DOI: 10.1021/acsami.7b17798
ACS Appl. Mater. Interfaces 2018, 10, 835−844

To resolve the instability problem of perovskite, tremendous efforts have been devoted, with significant advances achieved mostly based on doping chemicals in the perovskite layer, incorporating functional layers, and interface engineering between different layers (ETL, perovskite, and HTL).[20,25−28] Nevertheless, the real solution for this issue would rely on the understanding of the detailed mechanisms. In early research, composition of moisture, oxygen, and heat (sometimes with light too) was widely considered the main reason for decomposition of perovskite,[7,20,29] whereas counterexamples could also be found; for example, $MAPbI_3$ has shown stability in aqueous solution under certain conditions.[30] For ZnO, some preliminary research related the less stability of perovskite on ZnO to the existence of hydroxyl or acetate ligands in it.[31,32] More recently, studies have revealed a strong relationship between the perovskite instability and ion migration, which has also indicated that the moisture, oxygen, and heat might not be always necessary for the decomposition of perovskite.[33−36] For instance, different groups reported mass transport of extrinsic particles (Au) or ions (Li^+, etc.) from the adjacent layer into perovskite, which leads to degradation of the PSC.[35,37,38] In another research, Poglitsch and Weber reported that the $CH_3NH_3^+$ cation (MA^+) could not be fixed in the crystal structure because of the disordered orientation and mobility of the cation in the crystal.[39] Nevertheless, the factors that induce and influence the transport are still not clear, and a clear and consistent picture for those processes still remains unknown (key necessary parameters, species and their interactions, and any probable simple solutions), which requires more experimental and theoretical works for an answer.

In this work, we have discovered that perovskite could thermally decompose below the critical temperature that has been previously claimed to be stable. A perovskite sample placed above a hot plate has much faster degradation rate than that in an oven at the same temperature (100 °C), even with N_2 protection and isolation from light. A detailed experimental study that followed has revealed a decisive role of the temperature gradient in this phenomenon. It also proves that moisture and oxygen are not always necessary for the instability of perovskite. Further characterization has suggested a strong relationship of this phenomenon with the migration of ionic species driven by the temperature gradient other than thermal diffusion under a concentration gradient. Taking the example of perovskite/ZnO, the thermal transport of Zn^{2+} into the perovskite layer under an asymmetric temperature field can significantly influence the balance of the decomposition reaction of perovskite, so that its degradation process is greatly accelerated. We have found that such a process can be effectively suppressed when the temperature gradient was reduced by simple addition of a thermal reflector above the perovskite layer during the plate heating. Moreover, further experiments have shown that such a temperature gradient-driven chemical instability of perovskite widely exists in other perovskites (such as $FAPbI_3$) on various substrates (e.g., TiO_2, SnO_2, and PCBM (the short abbreviation for the fullerene derivative [6,6]-phenyl-C_{61}-butyric acid methyl ester)) as well and can also be physically suppressed by the reduction of the temperature gradient. This has proved the thermal migration of ions as an important factor for instability of perovskite in many previous studies and possible developments in the future. It has also suggested a simple but effective way of stabilizing PSCs regardless of detailed types of materials and systems.

2. EXPERIMENTAL SECTION

2.1. Preparation of Substrates. Fluorine-doped tin oxide (FTO) glass (Materwin, 14 $\Omega \cdot sq^{-1}$, 2.2 mm thick) was cleaned sequentially by ultrasonic bath with deionized water (18.2 MΩ·cm), acetone (Sinopharm, AR, ≥99.5%), isopropanol (Sinopharm, AR, ≥99.7%), and ethanol (Sinopharm, AR, ≥99.7%) for 30 min, dried with nitrogen (99.99%), and then cleaned by an ultraviolet-ozone cleaner (Hwotech, BZS250GF-TS). To prepare ZnO by the sol−gel (SG) method, a mixture was made with 0.15 M zinc acetate dehydrate [$Zn(CH_3COO)_2 \cdot 2H_2O$, Aladdin reagent, 99.995%] and 0.15 M diethanolamine (Aladdin reagent, ≥99.7%) in 1-butanol (Aladdin reagent, ≥99.7%). It was stirred until transparent and then aged for 24 h. Afterward, the solution was spin-coated onto FTO glass at 2000 rpm for 30 s in a spin coater (KW-4B, Jing Lin) three times, with heating on a hot plate (C-MAG HS7, IKA) at 120 °C for 5 min between each time. Finally, the products were transferred to a muffle oven (F48020-33-80CN, Thermo Scientific) and annealed at 350 °C for 1 h. ZnO was also fabricated by magnetron sputtering (MS) in a high vacuum chamber (CLUSTER-PECVD350, Xinlantian Technical) under 100 W ratio frequency sputtering for 7 min. The TiO_2 substrates were prepared by the spin-coating of 0.15 M titanium diisopropoxide bis(acetylacetonate) solution (Materwin, in 1-butanol) on the FTO glass under the same condition as that for ZnO and annealing at 500 °C for 15 min. For SnO_2, 0.15 M $SnCl_4 \cdot 5H_2O$ (Aldrich, 98%) was dissolved in 30 mL of ethanol (Sinopharm, AR, ≥99.7%) with stirring for 2 h to form the sol solution. After filtration, the solution was deposited on the FTO glass by three turns of spin-coating (3000 rpm, 30 s for each turn with heating on a hot plate at 120 °C for 5 min between each two turns) and then annealed in air at 450 °C in the oven for 10 min. The PCBM substrate was fabricated by spin-coating (2000 rpm for 30 s) with 30 mg mL^{-1} PCBM (Aldrich, 99.5%) chlorobenzene solution (from Materwin) on FTO and annealing at 100 °C on a hot plate for 20 min.

2.2. Fabrication and Treatment of Perovskite. For $MAPbI_3$, 60 μL of perovskite precursor solution [461 mg PbI_2 (Aldrich, 99.999%)], 159 mg of CH_3NH_3I (from Materwin), and 78 mg of dimethylsulfoxide (Aladdin reagent, ≥99.7%) dissolved in 600 mg of *N*,*N*-dimethylformamide (Aldrich, 99.8%) was spin-coated on ZnO (or TiO_2) at 4000 rpm for 30 s, with 0.5 mL of diethyl ether (Sinopharm, AR, ≥99.5%) being slowly dripped down in 10 s. For $FAPbI_3$, 60 μL of $FAPbI_3$ perovskite precursor solution (1.0 M, Materwin) was spin-coated on TiO_2 at 4000 rpm for 30 s. Both kinds of perovskite products were then placed in a N_2-protected glove chamber for 24 h until their colors turned to reddish brown. For instability experiments on perovskite, the samples were directly placed on a hot plate and a muffle oven with temperature already having reached 100 °C. For stability experiments on PSCs, the perovskite was annealed in the oven at 100 °C for 30 min.

2.3. Assembling of PSCs. For the growth of Spiro-OMeTAD, 73.3 mg of 2,20,7,70-tetrakis(*N*,*N*-di-*p*-methoxyphenylamino)-9,90-spirobiuorene (Materwin) in 1 mL of chlorobenzene was doped with 17.5 μL of Li-TFSI (520 mg mL^{-1} in acetonitrile) (Aladdin reagent, 99%) and 28.8 μL of 4-*tert*-butylpyridine (Aladdin reagent, 96%). Such a solution (50 μL) was spin-coated on the perovskite layer at 4000 rpm for 30 s. Finally, an 80 nm Au layer was deposited on the Spiro-OMeTAD layer by thermal evaporation. All PSCs were without encapsulation and any post-treatment.

2.4. Characterization of Materials and Devices. The morphological and structural analyses of the samples were investigated by a field-emission scanning electron microscope (Zeiss Ultra Plus) and an X-ray polycrystalline diffractometer (D8 ADVANCE Da Vinci, Bruker, Germany), respectively. The profile analysis was examined by time-of-flight secondary-ion mass spectrometry (ToF-SIMS, IonTOF, Germany). The real-time voltage measurement was done by an electronic sourcemeter (Keithley, 2400). The real-time temperature of the sample was detected by two infrared sensors (MI3, Raytek). The PSCs were characterized by standard procedures afterward.[40−42] The *J*−*V* characteristics were measured by a solar simulator (Newport, Oriel Sol-2A) under 1 sun

DOI: 10.1021/acsami.7b17798
ACS Appl. Mater. Interfaces 2018, 10, 835−844

(AM 1.5, 100 mW cm^{-2}) at room temperature (RT, 25 °C) with 10 samples under each condition. The scanning voltage was from −0.3 to 1.2 V (forward) and 1.2 to −0.3 V (reverse) with a rate of 100 mV s^{-1} and a 10 ms time delay. The size of PSCs was 2 × 2 cm^2, with an effective area of 0.15 cm^2 defined by a mask covered on top. A standard reference Si solar cell (effective area 2 × 2 cm^2, certified by VLSI Standards Inc.) was applied for the calibration of the simulator and calculation for the spectral mismatch, with a mismatch factor M = 1.003. The external quantum efficiency (EQE) spectrum was measured by a quantum efficiency/IPCE system (PV Measurements Inc., QEX10) in the wavelength range of 300−850 nm at RT.

3. RESULTS AND DISCUSSION

The temperature gradient-driven instability was first observed during our optimization experiment on the thermal treatment of perovskite on the ZnO substrate, and then systematic experiments were designed and carried out. First, ZnO substrates were fabricated by the SG method on the FTO glass, and then perovskite was grown on the substrates by one-step spin-coating.[43] The annealing processes were carried out on a programmable hot plate in a glove chamber and a muffle oven, separately, both set at 100 °C. To minimize the influence from the temperature ramping in the plate heating, the sample was only placed on the heating plate after the plate temperature had actually reached 100 °C. The setups were protected from the influence of moisture and oxygen by a N_2 atmosphere and isolated from light to exclude possible involvement of photocatalytic effect brought by the ZnO substrate. In the first method, the color of the sample started to change at 3 min and turned completely yellow in 5 min, as shown in Figure 1a,b (with the photograph shown in the inset). This result indicated significant decomposition of perovskite even with nitrogen protection under such a condition. In the second method, the perovskite remained black even after 1 h of continuous heating (Figure 1c), which means perovskite remained quite stable under this condition, though on the ZnO substrate that was previously considered to facilitate perovskite instability.[21,44] This quite distinctive behavior has been confirmed by the X-ray diffraction (XRD) results (Figure 1d). On the one hand, the peak position at 12.7° of the sample by plate heating was very similar to that of crystallized PbI_2 ([001] direction). On the other hand, the sample with oven heating for 1 h showed strong peaks at 14.1°, 20.1°, 28.7°, and 32.0°, corresponding to the [110], [112], [220], and [310] directions of the typical crystallized tetragonal perovskite, respectively. The different performance of the assembled PSCs shown in Figure 1e (for plate-heated and oven-heated samples, the η under reverse scanning are 13.3 and 1.1%, respectively; other parameters and EQE curves are in Table S1 and Figure S1 in the Supporting Information, respectively) also demonstrated the consequence that was induced by this effect.

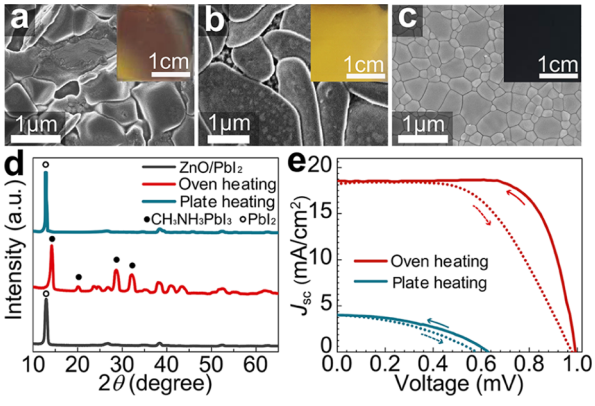

Figure 1. Effect of different heating methods on perovskite/ZnO. (a−c) Scanning electron microscope (SEM) images and real photographs of $CH_3NH_3PbI_3/ZnO_{SG}$ (a) heated on the hot plate (100 °C, 3 min), (b) heated on the hot plate (100 °C, 5 min), and (c) heated in the oven (100 °C, 1 h). (d) XRD patterns of PbI_2/ZnO (RT) and $CH_3NH_3PbI_3/ZnO_{SG}$ heated in the oven and on the hot plate. (e) J−V characteristics of the assembled PSCs.

According to some opinions from previous studies, the origin of the instability of perovskite on ZnO should be attributed to the reactions between perovskite and the contents of the substrate, for instance, the hydroxyl and acetate groups on the surface and in the bulk of the ZnO layer.[45−47] Therefore, a second experiment was carried out to evaluate the involvement of these species in the decomposition of perovskite in plate heating. The ZnO substrates were synthesized in two routes: (1) MS (with the ZnO substrate denoted as ZnO_{MS}) in vacuum to rule out the involvement of common ligands (OH− and COOH−); (2) SG method in air (the corresponding ZnO layer is denoted as ZnO_{SG}) for comparison. The result is shown in Figure 2. According to the SEM images, the surfaces of ZnO_{SG} and ZnO_{MS} appeared quite similar, and both were covered by many small inlands. For X-ray photoelectron spectroscopy (XPS) results, in ZnO_{SG}, the O 1s core level spectrum contains three peaks at 530.0, 531.2,

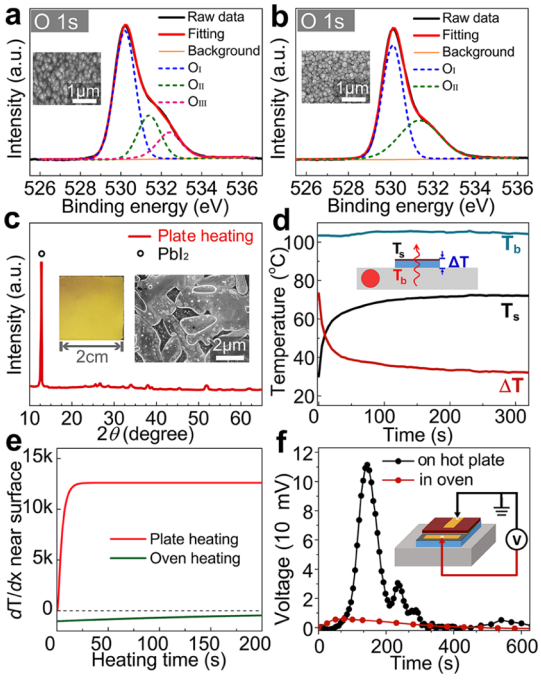

Figure 2. Further study on the thermal instability perovskite. (a,b) O 1s XPS core level spectra of ZnO_{SG} and ZnO_{MS}, respectively, with SEM images as insets. (c) XRD pattern, photograph, and SEM image of perovskite/ZnO_{MS} annealed on the hot plate (100 °C, 5 min). (d) Temperature vs time at different positions of the sample in the plate heating. (e) Simulation of the temperature gradient near the surface (~500 nm below the top surface) of the sample as the heating time increases. (f) Time dependence of voltage over the sample (taking the bottom as the positive position of the voltage and the upper side as grounded).

DOI: 10.1021/acsami.7b17798
ACS Appl. Mater. Interfaces 2018, 10, 835−844

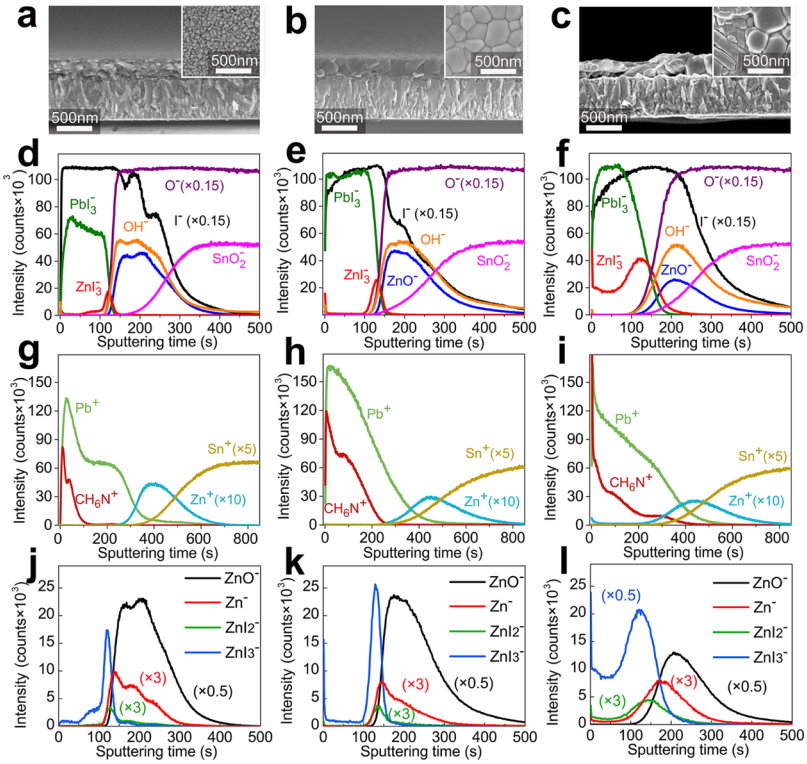

Figure 3. Detailed analysis on the formation and composition of $CH_3NH_3PbI_3$/ZnO under different heating conditions. (a–c) SEM of samples treated by (a) RT for 24 h; (b) oven heating, 100 °C, 1 h; (c) plate heating, 100 °C, 3 min (insets showing the top view). (d–f) SIMS results under conditions of (a–c), respectively, sputtered by Cs^+. (g–i) SIMS signals under conditions of (a–c), sputtered by O^{2-}. (j–l) Comparison of SIMS signals from Zn species under condition of (a–c), respectively, sputtered by Cs^+.

and 532.4 eV, corresponding to the Zn–O bond in the wurtzite structure and oxygen vacancies or defects in the presence of oxygen-deficient and chemisorbed functional groups such as hydroxyl and acetate ligands, respectively.[48,49] Meanwhile, no peak at 532.4 eV has been observed in ZnO_{MS}, which means no detectable existence of hydroxide and acetate ligands can be found, which is reasonable because the vacuum system contained only very little water vapor. However, the perovskite on ZnO_{MS} turned yellow soon after plate heating for about 5 min, with a distinct characteristic peak of PbI_2 in XRD (Figure 2c). The total survival time of perovskite on ZnO_{MG} was short similar to that on ZnO_{SG}, compared to the much longer survival time with oven heating (Figure 1c). Furthermore, stronger perovskite stability has been found onSG-fabricated TiO_2 (shown in Figure S2 in the Supporting Information), which also contains hydroxyl groups. Therefore, the chemisorbed groups (hydroxyl and acetate ligands, etc.) mentioned in previous reports are seemly not a decisive factor in this experiment.[23,47,50,51]

Because the samples were all identical with exclusion of the illumination and the chemical circumstance, the most probable factor that can cause such a difference should be the temperature distribution in the two heating systems. On the one hand, constant heating is symmetrically applied to the sample in the oven, so the temperature difference over the sample will soon become small after the heating started. On the other hand, constant heating is applied only from the bottom (plate), so the cold side always exists due to the dissipation to the atmosphere, and the temperature difference will be comparatively larger than that in the oven heating (can be seen from the experimental measurement shown in Figure 2d). We have also carried out some calculation on the detailed temperature distribution according to the basic model and the boundary temperature condition measured in the experiment (more detailed description can be found in Figure S3 in the Supporting Information). The calculated result also shows quite a high inhomogeneity in the plate heating but quite a homogeneous distribution in the oven. Moreover, the evolution of the temperature gradient (Figure 2e, at the depth of ~500 nm, close to the thickness of the perovskite and ZnO substrate) shows that the temperature gradient in plate heating very rapidly rises up to a high positive value (which means decreasing temperature from the bottom to the top), whereas it has only a much smaller negative value in the oven heating.

To study the exact effect that the asymmetry of heat brings to the perovskite stability, further work was carried out physically and chemically. The first suspected factor was the commonly known thermoelectric effect that exists on PN junctions or heterojunctions.[52,53] It means that this instability could have been possibly caused by electrochemical decomposition of perovskite influenced by the thermoelectric voltage of the heterojunctions in the perovskite/ZnO structure. So, a time-dependent series voltage measurement was carried out with an nV voltmeter under different conditions.[54,55] As shown in Figure 2f, the upper surface was grounded, and the voltage was measured at the FTO side. It can be seen that the voltage drop across the sample was positive in both cases. In the oven-heating, the U–t curve was quite flat, with the amplitude in the range of 10^{-2} mV through the heating process. On the contrary, under the plate-heating condition, there was a drastic increase of voltage at about 100 s and reached the maximum amplitude of around 1.1 mV at about 180 s. The emergence time of the voltage peak has been quite comparable to the one

DOI: 10.1021/acsami.7b17798
ACS Appl. Mater. Interfaces 2018, 10, 835–844

for the significant decomposition of perovskite by plate heating. It can be seen that even the highest value of voltage in the plate heating (10^0 mV) is much smaller than that is normally needed for the electrochemical decomposition of perovskite (normally in the range of 10^1 V), according to our previous research.[56] Therefore, the thermoelectric effect has seemly not been the main origin of this instability. Furthermore, as shown in Figure 2d, the temperature difference over the sample had a rapid decrease only in the initial 10 s and then became quite stable, much earlier than the emergence of the voltage peak. This nonsynchronized behavior indicates that the change in the temperature difference in general seems not to be the direct reason for the voltage peak. Instead, it may have been the consequence of other processes related to the decomposition reactions of perovskite under the influence of the temperature gradient. A more sound explanation for this might have been the collective motion of ionic species that were involved in the decomposition reactions of perovskite, according to some previous review works that have discussed the possibility of the perovskite instability generated by the ion-drifting processes.[29,57]

To investigate more details in this process, chemical analysis would be necessary to monitor the key difference between the two heating methods. Hence, ToF-SIMS was applied to detect the spatial distribution of chemical compounds after different heating processes by sputtering the sample with high-energy cesium and oxygen ion beams and analyzing the corresponding negatively and positively charged debris, respectively. The perovskite samples were taken after oven heating (100 °C) for 1 h and heterogeneous heating (100 °C) for 3 min. A control sample was prepared in the glove chamber for 24 h at RT for comparison. As shown in Figure 3a–c, the average size of grains is small in the RT sample but larger for the heated samples, which is a well-known effect that larger crystallized grains can be formed by higher activation energy induced by thermal heating.[58,59] For plate-heated samples, certain damage appears from the cross-sectional view. The distribution of the key components is presented in Figure 3d–f (sputtered by cesium) and Figure 3g–i (sputtered by oxygen). The sputtering time can be well-proportional to the depth of the sample that the ion beams has reached in different times of the sputtering, based on the principle of SIMS. On the basis of the distributions of PbI_3^-, ZnO^-, and SnO^-, the graphs can be divided into three zones corresponding to the spatial positions of the perovskite, ZnO, and FTO layers. Two significant phenomena could be noticed. First, compared to the samples with oven heating and without heating, the MA^+ ions penetrated much deeper into the layer of the ZnO in the sample with plate heating (if considering the sputtering rate constant, such depth was almost one-third of the ZnO thickness). Second, there are significantly stronger zinc iodide (ZnI_x^-, x = 1, 2, and 3) signals detected in the perovskite layer in the plate-heated sample, which can evidently prove the existence of ZnI^+, ZnI_2, and ZnI_3^- complexes, respectively.[60] It clearly indicates that there has been opposite migrations of zinc and MA species from the bottom-up and top-down directions, respectively. Moreover, taking a closer look, the distribution of ZnI_x species seemed to obey a certain sequence with increasing x index, as the distance is closer to the upper surface of perovskite (Figure 3j–l). It appeared that after ZnI^+ was formed (by reactions between the transported Zn^{2+} and I^-), they combined with more I^- to form ZnI_2 and then ZnI_3^- sequentially, as they approach the upper surface. Significant migration of alien species into the neighboring layers was detected in the plate-heating system, whereas no detectable trace of such a phenomenon can be observed in the homogeneous heating system or in the RT situation.

From the above results, we can try to draw a rough sketch of the mechanisms along with some theoretical explanations. As it is well-known, the particle flux in thermomigration can be described by equation (in one-dimensional system)[61,62]

$$J = J_d + J_m = -D\nabla_x C - \left(\frac{Q^* C}{RT^2}\right)\nabla_x T \quad (1)$$

where J is the total flux of particles, J_d is the part driven by diffusion from the concentration gradient, and J_m is the flux driven by the thermal gradient, together with Q^* the activation energy, D the diffusion coefficient, and C the particle concentration. In plate heating, there is always a hot side (FTO glass) by continuous heating from the bottom and a cold side (perovskite) by the dissipation process to the atmosphere, and therefore, the temperature gradient would be significant throughout the process. First, the Zn–O bond can be broken because of thermal excitation of Zn atoms by the heat coming from the hot side.[63] Second, these Zn^{2+} ions can be transported to the colder side, that is, the perovskite layer, and the flux will be proportional to the temperature gradient according to the second term of eq 1. One would naturally also notice the influence of the concentration gradient in the first term of eq 1. However, experiments have shown that the transporting process in the oven would be much weaker than on the plate, where the situation of the first term would be more or less similar. Therefore, the role of the concentration gradient in the comparison of two different heating methods would be accordingly much less important than the thermal gradient. According to the currently accepted opinion, the decomposition of perovskite consists of the following reactions[29,64]

$$CH_3NH_3PbI_3 \leftrightarrow CH_3NH_3I + PbI_2 \quad (2)$$

$$CH_3NH_3I \leftrightarrow CH_3NH_3^+ + I^- \quad (3)$$

Equations 2 and 3 stand for the decomposition of $MAPbI_3$ and MAI, respectively, which can take place subsequently in the normal decomposition process of perovskite. The invading Zn^{2+} ions can easily combine with I^- and thus accelerate the decomposition of MAI in the second step.[57,60,65] Therefore, the overall decomposition of perovskite would be accelerated. Zinc iodide can penetrate deeper into the perovskite and combine with more I^- ions when being driven by the thermal gradient. The production of zinc iodide species can be described as below[21]

$$xI^- + Zn^{2+} \rightarrow ZnI_x^{2-x} \quad (4)$$

In the meantime, the boosted perovskite dissociation can increase the production of the MA^+ cation. Such an increase of the MA^+ concentration can significantly enhance its diffusion into both the upper side of perovskite and the ZnO side and leave detectable traces in the SIMS spectroscopy that followed. Considering the positive sign of the voltage peak shown in Figure 2e and the dominance of ZnI_3^- in the zinc iodide species shown in Figure 3, the main content of the ionic current is likely the MA^+ cation that moves from the top to the bottom, and ZnI_3^- from the bottom to the top. Moreover, according to the second term in eq 1, the thermomigration is

DOI: 10.1021/acsami.7b17798
ACS Appl. Mater. Interfaces 2018, 10, 835–844

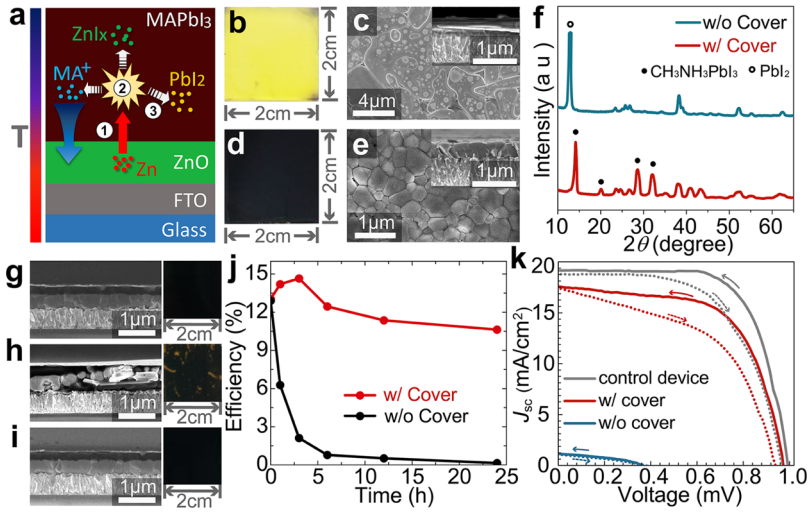

Figure 4. Stabilization of perovskite and assembled PSCs by reducing the temperature gradient: (a) Brief description of the decomposition mechanism. (b) Photograph and (c) SEM of the sample heated on the hot plate at 100 °C without cover. (d) Photograph and (e) SEM of sample heated on the hot plate at 100 °C with aluminum foil cover. (f) XRD of samples without and with Al cover. (g) SEM and real photograph of PSC before the stability test. (h,i) PSCs being heated on the hot plate at 100 °C for 3 h without and with Al cover, respectively. (j) Efficiency of PSCs vs heating time. (k) $J-V$ characteristics of PSCs with and without Al cover heated at 100 °C for 24 h (control device was kept at RT for 24 h).

also proportional to the local concentration of transported species. Because the bonding energy of the Zn−O (≤226 kJ mol^{-1}) bond is much smaller than that of the Ti−O (666.5 kJ mol^{-1}) bond, the decomposition process in the TiO_2 substrate would be much weaker.[63,66] Therefore, the thermomigration of ionic species by the temperature gradient would be smaller in TiO_2, which explains the relatively higher stability of perovskite/TiO_2 under the same condition (as can be seen in Figure S2). Moreover, the activation energy and the temperature are also noticeable factors in the same term. Hence, altering the structural parameter of the substrate material, changing its chemical composition, or tuning the ambient temperature may also influence the thermal stability of perovskite-on-substrate in this aspect.

From the above discussion, we can more or less conclude the relationship of the significant instability of perovskite/ZnO for enhancement of ion migration induced by the temperature gradient. To confirm this, an experiment was further carried out to investigate the consequence of suppressing the temperature gradient. As is well-known, Al foil can effectively reflect infrared radiation and therefore increase the temperature of the atmosphere nearby. In this experiment, an Al foil was simply fixed on top of a sample, and then the whole setup (shown in Figure S4 in the Supporting Information) was heated on the hot plate. A control experiment was also carried out without the Al cover on top of the perovskite. As shown in Figure 4, on the one hand, the sample without the Al cover turned yellow in 5 min. On the other hand, the perovskite with the Al cover on top remained entirely black even after 30 min. According to the SEM images, certain damage emerged in the sample without the cover, whereas the one with the Al cover was still quite uniform. The XRD in Figure 4f shows a significant peak at 14.1°, 20.1°, 28.7°, and 32.0° but with the absence of peak at 12.7° (corresponding to PbI_2) in the second sample. This result has clearly shown much improved stability of crystallized perovskite by simply utilizing the Al foil as a simple heat reflector into the system. Besides, it has confirmed again the important role of temperature gradient in the instability of perovskite and its dominant influence in the transport process, compared to the concentration gradient-driven diffusion, as discussed in eq 1.

Nevertheless, in real application, though the stability of perovskite may also be improved using oven heating during the fabrication stage (Figure 1), a significant temperature gradient can widely exist in the solar cells under sunlight illumination. Therefore, we also carried out similar experiments on PSCs (with classical FTO/ZnO/$CH_3NH_3PbI_3$/Spiro-MeOTAD/Au architecture). The PSCs were heated on the 100 °C hot plate in the glove chamber in the N_2 atmosphere without and with Al cover on top. The $J-V$ characteristics were taken at different time stages in 24 h, with the representative result shown in Figure 4k (more statistical details can be found in Tables S2−S4 and Figure S5 in the Supporting Information). The test was run ten times for each condition to be more statistically certain. For identical comparison (Al cover can block some light), both heating processes were isolated from illumination. For the PSC without the Al cover, the sample began to turn yellow in the first 30 min. In 3 h, the perovskite layer was significantly damaged in continuity and uniformity, whereas several significant yellow regions appeared in the sample (Figure 4h). Meanwhile, the PSC with the Al cover had nearly no significant change either in the morphology or color. For conversion efficiency, on the one hand, the PSC without the cover showed drastic degradation versus time, with η dropped over 50% after the first hour and to almost zero after 24 h. On the other hand, the PSC with the cover has even showed an initial increase of conversion efficiency in 3 h and then quite a slow degradation. As shown in Figure 4k, the PSC built on ZnO still retained the efficiency of 10.6% (77.4% of initial value) even after 100 °C heating treatment for 24 h. This experiment has also shown that the temperature gradient-induced thermal instability also exists in annealed crystalline perovskite, though with a longer lifetime compared to the one without annealing, as shown in the result in Figure 1. Beside better crystalline conditions, the longer lifetime in PSCs could also have been facilitated by the blocking effect on the heat and leakage of MA by the HTL layer and the glass above it.

DOI: 10.1021/acsami.7b17798
ACS Appl. Mater. Interfaces 2018, 10, 835−844

Until now, we have discussed the situations for perovskite on the ZnO substrate. In the current research, other candidates have been more frequently used because of their better stability (such as TiO_2, SnO_2, and PCBM), though normally more expensive than ZnO.[67] Therefore, similar instability experiments have also been performed on these three mainstream ETL substrates. As widely known, the performance of perovskite is very sensitive to the inhomogeneity inside it, so the time when the perovskite layer turned yellow (corresponding to the decomposition of perovskite and formation of PbI_2) is an adequate critical point for instability of perovskite, no matter how large the yellow area is. The results are listed in Table 1 (detailed photographs of the time series experiment

Table 1. Thermal Stability of Perovskite Films on Mainstream Substrates under Different Conditions[a]

method		ZnO	TiO_2 (h)	SnO_2 (h)	$PC_{60}BM$ (h)
hot plate heating	without cover	3 min	4	2	3
	with cover	45 min	>32	28	32
oven heating		2.5 h	>32	>32	>32

[a]The stability is represented by the time it takes for the emergence of yellow color in the sample heated at 100 °C, with N_2 protection and isolation from illumination.

can be found in Figures S6−S8 in the Supporting Information). It can be seen that the distinctive stability of perovskite depending on the heating methods can exist on TiO_2, SnO_2, and PCBM. On the hot plate, the survival time of perovskite is almost 1 order of magnitude shorter than in the oven. Furthermore, the addition of the heat-reflecting cover on top of the perovskite can also significantly enhance its stability on those substrates. Such experiments have further proved that the temperature gradient-induced instability can take place on almost all mainstream ETL substrates. In those processes, the mass transport of particles (however, the type of transported particle will depend on the detailed substrate) would also play an important role in the generation of instability. What is more, we also performed the stability test of $FAPbI_3$ on the TiO_2 substrate and discovered a similar phenomenon, where $FAPbI_3$ decomposed in only 5 min on the hot plate but remained almost unchanged in 3 h in the oven (details can be found in Figure S9 in the Supporting Information). Meanwhile, the addition of the thermal reflection cover could significantly stabilize it on the hot plate (lifetime >30 min). It further supported that such an instability can take place on other types of perovskite as well if they chemically follow a similar way of decomposition like $MAPbI_3$ and could also be stabilized by simply reducing the temperature gradient. Predictably, such phenomena may also very probably exist in the more recently developed p−i−n-structured perovskite solar cells, with the perovskite layer grown on HTLs, and could be even stronger than that on ETLs because of their (NiO_x, CuS, CuSCN, PEDOT:PSS, etc.) good ionic-transporting ability.[68−71]

Finally, according to this investigation, there are the following key processes involved in the stability of perovskite: (1) existence of ions or neutral particles that can enhance the decomposition of perovskite, which could have already existed or be generated by intrinsic or thermoexcitation in the layers adjacent to perovskite; (2) effective mass transport of such species in the adjacent layer through the interfaces and then into the perovskite layer; and (3) reaction of such species with the local perovskite. To stabilize the perovskite, one can either avoid the generation of deteriorating particles adjacent to perovskite, block the pathway of mass transport, lower the mobility of particles, reduce the force that drives the transport, or weaken the reaction of those species with local perovskite. Looking back into all stabilization efforts on the perovskite, the above routes have been normally realized by passivation of perovskite by chemical doping and blockage effect by interface engineering.[22,23,31,46,51,57,72,73] Nevertheless, perhaps it will also be a good trial to stabilize the perovskite by weakening the transport itself, according to this paper.

4. CONCLUSIONS

In conclusion, this work has proved the existence of a new type of chemical instability of perovskite, caused by the temperature gradient, and studied its origin and detailed mechanism. Temperature gradient can greatly deteriorate the stability of the as-formed perovskite and the crystalline one in PSCs at low temperature even with protection from moisture, oxygen, and light, whereas the hydroxyl and acetate groups near the interface or the direct reaction with the adjacent layer are seemly not necessary conditions for the perovskite instability. Further mechanism study has revealed that the temperature gradient appeared as the main driving force for the mass transport of extrinsic ionic species relevant to the decomposition reaction of perovskite from the neighboring layers. Moreover, we have proved the significant enhancement of the stability of perovskite by reducing the temperature gradient with the addition of a covering structure. In the perovskite/ZnO system, the survival time extended from 2−3 min to 1 order of magnitude longer at 100 °C heating in air and has shown even better effect in the application of PSCs. Eventually, the universality of such a phenomenon has also been found existing in many other systems with various perovskites and ETL substrates, and predictably may also exist with HTL substrates (NiO_x, CuS, CuSCN, PEDOT:PSS, etc.). In general, this work may give some light to the study on the stabilization of perovskite and the development of applicable perovskite devices via different approaches.

■ ASSOCIATED CONTENT

Supporting Information

The Supporting Information is available free of charge on the ACS Publications website at DOI: 10.1021/acsami.7b17798.

Voltage value between the TiO_2 layer and the perovskite layer versus time under different heating conditions; stability experiment of perovskite on TiO_2 substrates and the corresponding analysis; approximate simulation of temperature distribution for samples; schematic illustration of the experimental setup for reducing the temperature gradient; stability test of $MAPbI_3$ on TiO_2, SnO_2, and PCBM and of $FAPbI_3$ on TiO_2, current density−voltage characteristics of each treatment (PDF)

■ AUTHOR INFORMATION

Corresponding Authors

*E-mail: liuhong@sjtu.edu.cn (H.L.).
*E-mail: wzshen@sjtu.edu.cn (W.S.).

ORCID

Hong Liu: 0000-0002-2241-1199

DOI: 10.1021/acsami.7b17798
ACS Appl. Mater. Interfaces 2018, 10, 835−844

Author Contributions

[§]X.W. and H.L. contributed equally to this work.

Notes

The authors declare no competing financial interest.

■ ACKNOWLEDGMENTS

This work was supported by the Natural Science Foundation of China (61234005, 11204176, and 11474201), the National Major Basic Research Project (2012CB934302), and the Fundamental Research Funds for the Central Universities from the Ministry of Education (China).

■ REFERENCES

(1) Stranks, S. D.; Snaith, H. J. Metal-Halide Perovskites for Photovoltaic and Light-Emitting Devices. *Nat. Nanotechnol.* **2015**, *10*, 391−402.
(2) Green, M. A.; Ho-Baillie, A.; Snaith, H. J. The Emergence of Perovskite Solar Cells. *Nat. Photonics* **2014**, *8*, 506−514.
(3) Zhao, Y.; Zhu, K. Organic-Inorganic Hybrid Lead Halide Perovskites for Optoelectronic and Electronic Applications. *Chem. Soc. Rev.* **2016**, *45*, 655−689.
(4) Park, N.-G.; Grätzel, M.; Miyasaka, T.; Zhu, K.; Emery, K. Towards Stable and Commercially Available Perovskite Solar Cells. *Nat. Energy* **2016**, *1*, 16152.
(5) Hadadian, M.; Correa-Baena, J.-P.; Goharshadi, E. K.; Ummadisingu, A.; Seo, J.-Y.; Luo, J.; Gholipour, S.; Zakeeruddin, S. M.; Saliba, M.; Abate, A.; Grätzel, M.; Hagfeldt, A. Enhancing Efficiency of Perovskite Solar Cells via N-doped Graphene: Crystal Modification and Surface Passivation. *Adv. Mater.* **2016**, *28*, 8681−8686.
(6) Saliba, M.; Matsui, T.; Domanski, K.; Seo, J.-Y.; Ummadisingu, A.; Zakeeruddin, S. M.; Correa-Baena, J.-P.; Tress, W. R.; Abate, A.; Hagfeldt, A.; Grätzel, M. Incorporation of Rubidium Cations Into Perovskite Solar Cells Improves Photovoltaic Performance. *Science* **2016**, *354*, 206−209.
(7) Wang, D.; Wright, M.; Elumalai, N. K.; Uddin, A. Stability of Perovskite Solar Cells. *Sol. Energy Mater. Sol. Cells* **2016**, *147*, 255−275.
(8) Pan, J.; Mu, C.; Li, Q.; Li, W.; Ma, D.; Xu, D. Room-Temperature, Hydrochloride-Assisted, One-Step Deposition for Highly Efficient and Air-Stable Perovskite Solar Cells. *Adv. Mater.* **2016**, *28*, 8309−8314.
(9) Yang, S.; Fu, W.; Zhang, Z.; Chen, H.; Li, C.-Z. Recent Advances in Perovskite Solar Cells: Efficiency, Stability and Lead-Free Perovskite. *J. Mater. Chem. A* **2017**, *5*, 11462−11482.
(10) Wang, Z.; McMeekin, D. P.; Sakai, N.; van Reenen, S.; Wojciechowski, K.; Patel, J. B.; Johnston, M. B.; Snaith, H. J. Efficient and Air-Stable Mixed-Cation Lead Mixed-Halide Perovskite Solar Cells with N-doped Organic Electron Extraction Layers. *Adv. Mater.* **2017**, *29*, 1604186.
(11) Luo, P.; Liu, Z.; Xia, W.; Yuan, C.; Cheng, J.; Lu, Y. A Simple in situ Tubular Chemical Vapor Deposition Processing of Large-Scale Efficient Perovskite Solar Cells and the Research on Their Novel Roll-Over Phenomenon in J−V Curves. *J. Mater. Chem. A* **2015**, *3*, 12443−12451.
(12) Saliba, M.; Matsui, T.; Seo, J.-Y.; Domanski, K.; Correa-Baena, J.-P.; Nazeeruddin, M. K.; Zakeeruddin, S. M.; Tress, W.; Abate, A.; Hagfeldt, A.; Grätzel, M. Cesium-Containing Triple Cation Perovskite Solar Cells: Improved Stability, Reproducibility and High Efficiency. *Energy Environ. Sci.* **2016**, *9*, 1989−1997.
(13) Cacovich, S.; Ciná, L.; Matteocci, F.; Divitini, G.; Midgley, P. A.; Di Carlo, A.; Ducati, C. Gold and Iodine Diffusion in Large Area Perovskite Solar Cells under Illumination. *Nanoscale* **2017**, *9*, 4700−4706.
(14) Baranwal, A. K.; Kanaya, S.; Peiris, T. A. N.; Mizuta, G.; Nishina, T.; Kanda, H.; Miyasaka, T.; Segawa, H.; Ito, S. 100 °C Thermal Stability of Printable perovskite Solar Cells Using Porous Carbon Counter Electrodes. *ChemSusChem* **2016**, *9*, 2604−2608.
(15) Zhao, X.; Kim, H.-S.; Seo, J.-Y.; Park, N.-G. Effect of Selective Contacts on the Thermal Stability of Perovskite Solar Cells. *ACS Appl. Mater. Interfaces* **2017**, *9*, 7148−7153.
(16) Hsu, H.-L.; Chen, C.-P.; Chang, J.-Y.; Yu, Y.-Y.; Shen, Y.-K. Two-Step Thermal Annealing Improves the Morphology of Spin-Coated Films for Highly Efficient Perovskite Hybrid Photovoltaics. *Nanoscale* **2014**, *6*, 10281−10288.
(17) Eperon, G. E.; Burlakov, V. M.; Docampo, P.; Goriely, A.; Snaith, H. J. Morphological Control for High Performance, Solution-Processed Planar Heterojunction Perovskite Solar Cells. *Adv. Funct. Mater.* **2014**, *24*, 151−157.
(18) van Reenen, S.; Kemerink, M.; Snaith, H. J. Modeling Anomalous Hysteresis in Perovskite Solar Cells. *J. Phys. Chem. Lett.* **2015**, *6*, 3808−3814.
(19) Snaith, H. J.; Abate, A.; Ball, J. M.; Eperon, G. E.; Leijtens, T.; Noel, N. K.; Stranks, S. D.; Wang, J. T.-W.; Wojciechowski, K.; Zhang, W. Anomalous Hysteresis in Perovskite Solar Cells. *J. Phys. Chem. Lett.* **2014**, *5*, 1511−1515.
(20) Niu, G.; Guo, X.; Wang, L. Review of Recent Progress in Chemical Stability of Perovskite Solar Cells. *J. Mater. Chem. A* **2015**, *3*, 8970−8980.
(21) Dkhissi, Y.; Meyer, S.; Chen, D.; Weerasinghe, H. C.; Spiccia, L.; Cheng, Y.-B.; Caruso, R. A. Stability Comparison of Perovskite Solar Cells Based on Zinc Oxide and Titania on Polymer Substrates. *ChemSusChem* **2016**, *9*, 687−695.
(22) Mahmood, K.; Swain, B. S.; Amassian, A. 16.1% Efficient Hysteresis-Free Mesostructured Perovskite Solar Cells Based on Synergistically Improved ZnO Nanorod Arrays. *Adv. Energy Mater.* **2015**, *5*, 1500568.
(23) Wang, P.; Zhao, J.; Liu, J.; Wei, L.; Liu, Z.; Guan, L.; Cao, G. Stabilization of Organometal Halide Perovskite Films by SnO_2 Coating with Inactive Surface Hydroxyl Groups on ZnO Nanorods. *J. Power Sources* **2017**, *339*, 51−60.
(24) Manspeaker, C.; Scruggs, P.; Preiss, J.; Lyashenko, D. A.; Zakhidov, A. A. Reliable Annealing of $CH_3NH_3PbI_3$Films Deposited on ZnO. *J. Phys. Chem. C* **2016**, *120*, 6377−6382.
(25) Tan, H.; Jain, A.; Voznyy, O. Efficient and Stable Solution-Processed Planar Perovskite Solar Cells via Contact Passivation. *Science* **2017**, *355*, 722−726.
(26) Zhang, H.; Shi, Y.; Yan, F.; Wang, L.; Wang, K.; Xing, Y.; Dong, Q.; Ma, T. A Dual Functional Additive for The HTM Layer in Perovskite Solar cells. *Chem. Commun.* **2014**, *50*, 5020−5022.
(27) Zuo, L.; Gu, Z.; Ye, T.; Fu, W.; Wu, G.; Li, H.; Chen, H. Enhanced Photovoltaic Performance of $CH_3NH_3PbI_3$ Perovskite Solar Cells through Interfacial Engineering Using Self-Assembling Monolayer. *J. Am. Chem. Soc.* **2015**, *137*, 2674−2679.
(28) Zhang, Y.; Fei, Z.; Gao, P.; Lee, Y.; Tirani, F. F.; Scopelliti, R.; Feng, Y.; Dyson, P. J.; Nazeeruddin, M. K. A Strategy to Produce High Efficiency, High Stability Perovskite Solar Cells Using Functionalized Ionic Liquid-Dopants. *Adv. Mater.* **2017**, *29*, 1702157.
(29) Leijtens, T.; Eperon, G. E.; Noel, N. K.; Habisreutinger, S. N.; Petrozza, A.; Snaith, H. J. Stability of Metal Halide Perovskite Solar Cells. *Adv. Energy Mater.* **2015**, *5*, 1500963.
(30) Park, S.; Chang, W. J.; Lee, C. W.; Park, S.; Ahn, H.-Y.; Nam, K. T. Photocatalytic Hydrogen Generation from Hydriodic Acid Using Methylammonium Lead Iodide in Dynamic Equilibrium with Aqueous Solution. *Nat. Energy* **2016**, *2*, 16185.
(31) Cheng, Y.; Yang, Q.-D.; Xiao, J.; Xue, Q.; Li, H.-W.; Guan, Z.; Yip, H.-L.; Tsang, S.-W. Decomposition of Organometal Halide Perovskite Films on Zinc Oxide Nanoparticles. *ACS Appl. Mater. Interfaces* **2015**, *7*, 19986−19993.
(32) Yang, J.; Siempelkamp, B. D.; Mosconi, E.; De Angelis, F.; Kelly, T. L. Origin of the Thermal Instability in $CH_3NH_3PbI_3$ Thin Films Deposited on ZnO. *Chem. Mater.* **2015**, *27*, 4229−4236.
(33) Miyano, K.; Yanagida, M.; Tripathi, N.; Shirai, Y. Hysteresis, Stability, and Ion Migration in Lead Halide Perovskite Photovoltaics. *J. Phys. Chem. Lett.* **2016**, *7*, 2240−2245.

DOI: 10.1021/acsami.7b17798
ACS Appl. Mater. Interfaces 2018, 10, 835−844

(34) Yuan, Y.; Huang, J. Ion Migration in Organometal Trihalide Perovskite and Its Impact on Photovoltaic Efficiency and Stability. *Acc. Chem. Res.* **2016**, *49*, 286−293.
(35) Li, Z.; Xiao, C.; Yang, Y.; Harvey, S. P.; Kim, D. H.; Christians, J. A.; Yang, M.; Schulz, P.; Nanayakkara, S. U.; Jiang, C.-S.; Luther, J. M.; Berry, J. J.; Beard, M. C.; Al-Jassim, M. M.; Zhu, K. Extrinsic Ion Migration in Perovskite Solar Cells. *Energy Environ. Sci.* **2017**, *10*, 1234−1242.
(36) Yuan, H.; Debroye, E.; Janssen, K.; Naiki, H.; Steuwe, C.; Lu, G.; Moris, M.; Orgiu, E.; Uji-i, H.; De Schryver, F.; Samorì, P.; Hofkens, J.; Roeffaers, M. Degradation of Methylammonium Lead Iodide Perovskite Structures through Light and Electron Beam Driven Ion Migration. *J. Phys. Chem. Lett.* **2016**, *7*, 561−566.
(37) Domanski, K.; Correa-Baena, J.-P.; Mine, N.; Nazeeruddin, M. K.; Abate, A.; Saliba, M.; Tress, W.; Hagfeldt, A.; Grätzel, M. Not All That Glitters Is Gold: Metal-Migration-Induced Degradation in Perovskite Solar Cells. *ACS Nano* **2016**, *10*, 6306−6314.
(38) Hawash, Z.; Ono, L. K.; Raga, S. R.; Lee, M. V.; Qi, Y. Air-Exposure Induced Dopant Redistribution and Energy Level Shifts in Spin-Coated Spiro-MeOTAD Films. *Chem. Mater.* **2015**, *27*, 562−569.
(39) Poglitsch, A.; Weber, D. Dynamic Disorder in Methylammoniumtrihalogenoplumbates (II) Observed by Millimeter-Wave Spectroscopy. *J. Chem. Phys.* **1987**, *87*, 6373−6378.
(40) Christians, J. A.; Manser, J. S.; Kamat, P. V. Best Practices in Perovskite Solar Cell Efficiency Measurements. Avoiding the Error of Making Bad Cells Look Good. *J. Phys. Chem. Lett.* **2015**, *6*, 852−857.
(41) Timmreck, R.; Meyer, T.; Gilot, J.; Seifert, H.; Mueller, T.; Furlan, A.; Wienk, M. M.; Wynands, D.; Hohl-Ebinger, J.; Warta, W.; Janssen, R. A. J.; Riede, M.; Leo, K. Characterization of Tandem Organic Solar Cells. *Nat. Photonics* **2015**, *9*, 478−479.
(42) Luber, E. J.; Buriak, J. M. Reporting Performance in Organic Photovoltaic Devices. *ACS Nano* **2013**, *7*, 4708−4714.
(43) Ahn, N.; Son, D.-Y.; Jang, I.-H.; Kang, S. M.; Choi, M.; Park, N.-G. Highly Reproducible Perovskite Solar Cells with Average Efficiency of 18.3% and Best Efficiency of 19.7% Fabricated via Lewis Base Adduct of Lead(II) Iodide. *J. Am. Chem. Soc.* **2015**, *137*, 8696−8699.
(44) Song, J.; Hu, W.; Wang, X.-F.; Chen, G.; Tian, W.; Miyasaka, T. $HC(NH_2)_2PbI_3$ as a Thermally Stable Absorber for Efficient ZnO-Based Perovskite Solar Cells. *J. Mater. Chem. A* **2016**, *4*, 8435−8443.
(45) Song, J.; Zheng, E.; Wang, X.-F.; Tian, W.; Miyasaka, T. Low-Temperature-Processed ZnO−SnO 2 Nanocomposite for Efficient Planar Perovskite Solar Cells. *Sol. Energy Mater. Sol. Cells* **2016**, *144*, 623−630.
(46) Si, H.; Liao, Q.; Zhang, Z.; Li, Y.; Yang, X.; Zhang, G.; Kang, Z.; Zhang, Y. An Innovative Design of Perovskite Solar Cells with Al_2O_3 Inserting at ZnO/Perovskite Interface for Improving the Performance and Stability. *Nano Energy* **2016**, *22*, 223−231.
(47) Zhao, X.; Shen, H.; Zhang, Y.; Li, X.; Zhao, X.; Tai, M.; Li, J.; Li, J.; Li, X.; Lin, H. Aluminum-Doped Zinc Oxide as Highly Stable Electron Collection Layer for Perovskite Solar Cells. *ACS Appl. Mater. Interfaces* **2016**, *8*, 7826−7833.
(48) Tseng, Z.-L.; Chiang, C.-H.; Wu, C.-G. Surface Engineering of ZnO Thin Film for High Efficiency Planar Perovskite Solar Cells. *Sci. Rep.* **2015**, *5*, 13211.
(49) Zhang, X.; Qin, J.; Xue, Y.; Yu, P.; Zhang, B.; Wang, L.; Liu, R. Effect of Aspect Ratio and Surface Defects on the Photocatalytic Activity of ZnO Nanorods. *Sci. Rep.* **2014**, *4*, 4596.
(50) Qin, F.; Meng, W.; Fan, J.; Ge, C.; Luo, B.; Ge, R.; Hu, L.; Jiang, F.; Liu, T.; Jiang, Y.; Zhou, Y. Enhanced Thermochemical Stability of $CH_3NH_3PbI_3$ Perovskite Films on Zinc Oxides via New Precursors and Surface Engineering. *ACS Appl. Mater. Interfaces* **2017**, *9*, 26045−26051.
(51) Tavakoli, M. M.; Tavakoli, R.; Nourbakhsh, Z.; Waleed, A.; Virk, U. S.; Fan, Z. High Efficiency and Stable Perovskite Solar Cell Using ZnO/rGO QDs as an Electron Transfer Layer. *Adv. Mater. Interfaces* **2016**, *3*, 1500790.
(52) Rowe, D. M. *CRC Handbook of Thermoelectrics*, 1st ed.; CRC Press: NY, USA, 1995.
(53) Burke, P. G.; Curtin, B. M.; Bowers, J. E.; Gossard, A. C. Minority Carrier Barrier Heterojunctions for Improved Thermoelectric Efficiency. *Nano Energy* **2015**, *12*, 735−741.
(54) Wagner, M.; Span, G.; Holzer, S.; Grasser, T. Thermoelectric Power Generation Using Large-Area Si/SiGe pn-Junctions with Varying Ge Content. *Semicond. Sci. Technol.* **2007**, *22*, S173−S176.
(55) Chavez, R.; Angst, S.; Hall, J.; Stoetzel, J.; Kessler, V.; Bitzer, L.; Maculewicz, F.; Benson, N.; Wiggers, H.; Wolf, D.; Schierning, G.; Schmechel, R. High Temperature Thermoelectric Device Concept Using Large Area PN Junctions. *J. Electron. Mater.* **2014**, *43*, 2376−2383.
(56) Zhou, F.; Liu, H.; Wang, X.; Shen, W. Fast and Controllable Electric-Field-Assisted Reactive Deposited Stable and Annealing-Free Perovskite toward Applicable High-Performance Solar Cells. *Adv. Funct. Mater.* **2017**, *27*, 1606156.
(57) Back, H.; Kim, G.; Kim, J.; Kong, J.; Kim, T. K.; Kang, H.; Kim, H.; Lee, J.; Lee, S.; Lee, K. Achieving Long-Term Stable Perovskite Solar Cells via Ion Neutralization. *Energy Environ. Sci.* **2016**, *9*, 1258−1263.
(58) Ye, J.; Zheng, H.; Zhu, L.; Zhang, X.; Jiang, L.; Chen, W.; Liu, G.; Pan, X.; Dai, S. High-Temperature Shaping Perovskite Film Crystallization for Solar Cell Fast Preparation. *Sol. Energy Mater. Sol. Cells* **2017**, *160*, 60−66.
(59) Ke, J.-C.; Wang, Y.-H.; Chen, K.-L.; Huang, C.-J. Effect of Temperature Annealing Treatments and Acceptors in $CH_3NH_3PbI_3$ Perovskite Solar Cell Fabrication. *J. Alloys Compd.* **2017**, *695*, 2453−2457.
(60) Wakita, H.; Johansson, G.; Sandström, M.; Goggin, P. L.; Ohtaki, H. Structure Determination of Zinc Iodide Complexes in Aqueous Solution. *J. Solution Chem.* **1991**, *20*, 643−668.
(61) Richard, J. B.; Dienes, G. J. *An Introduction to Solid State Diffusion*, 1st ed.; Academic Press: NY, USA, 1988.
(62) LeClaire, A. D. Some Predicted Effects of Temperature Gradients on Diffusion in Crystals. *Phys. Rev.* **1954**, *93*, 344.
(63) Watson, L. R.; Thiem, T. L.; Dressler, R. A.; Salter, R. H.; Murad, E. High Temperature Mass Spectrometric Studies of the Bond Energies of Gas-Phase Zinc Oxide, Nickel Oxide, and Copper(II) Oxide. *J. Phys. Chem.* **1993**, *97*, 5577−5580.
(64) Azpiroz, J. M.; Mosconi, E.; Bisquert, J.; De Angelis, F. Defect Migration in Methylammonium Lead Iodide and Its Role in Perovskite Solar Cell Operation. *Energy Environ. Sci.* **2015**, *8*, 2118−2127.
(65) Li, B.; Nie, Z.; Vijayakumar, M.; Li, G.; Liu, J.; Sprenkle, V.; Wang, W. Ambipolar Zinc-Polyiodide Electrolyte for a High-Energy Density Aqueous Redox Flow Battery. *Nat. Commun.* **2015**, *6*, 6303.
(66) Luo, Y.-R. *Comprehensive Handbook of Chemical Bond Energies*, 1st ed.; CRC Press: NY, USA, 2007.
(67) Li, F.; Liu, M. Recent Efficient Strategies for Improving the Moisture Stability of Perovskite Solar Cells. *J. Mater. Chem. A* **2017**, *5*, 15447−15459.
(68) Bai, Y.; Chen, H.; Xiao, S.; Xue, Q.; Zhang, T.; Zhu, Z.; Li, Q.; Hu, C.; Yang, Y.; Hu, Z.; Huang, F.; Wong, K. S.; Yip, H.-L.; Yang, S. Effects of a Molecular Monolayer Modification of NiO Nanocrystal Layer Surfaces on Perovskite Crystallization and Interface Contact toward Faster Hole Extraction and Higher Photovoltaic Performance. *Adv. Funct. Mater.* **2016**, *26*, 2950−2958.
(69) Zhao, L.; Luo, D.; Wu, J.; Hu, Q.; Zhang, W.; Chen, K.; Liu, T.; Liu, Y.; Zhang, Y.; Liu, F.; Russell, T. P.; Snaith, H. J.; Zhu, R.; Gong, Q. High-Performance Inverted Planar Heterojunction Perovskite Solar Cells Based on Lead Acetate Precursor with Efficiency Exceeding 18%. *Adv. Funct. Mater.* **2016**, *26*, 3508−3514.
(70) Ye, S.; Sun, W.; Li, Y.; Yan, W.; Peng, H.; Bian, Z.; Liu, Z.; Huang, C. CuSCN-Based Inverted Planar Perovskite Solar Cell with an Average PCE of 15.6%. *Nano Lett.* **2015**, *15*, 3723−3728.
(71) Rao, H.; Sun, W.; Ye, S.; Yan, W.; Li, Y.; Peng, H.; Liu, Z.; Bian, Z.; Huang, C. Solution-Processed CuS NPs as an Inorganic Hole-

DOI: 10.1021/acsami.7b17798
ACS Appl. Mater. Interfaces 2018, 10, 835−844

Selective Contact Material for Inverted Planar Perovskite Solar Cells. *ACS Appl. Mater. Interfaces* **2016**, *8*, 7800−7805.
(72) Yin, X.; Xu, Z.; Guo, Y.; Xu, P.; He, M. Ternary Oxides in the TiO_2-ZnO System as Efficient Electron-Transport Layers for Perovskite Solar Cells with Efficiency over 15%. *ACS Appl. Mater. Interfaces* **2016**, *8*, 29580−29587.
(73) Tseng, Z.-L.; Chiang, C.-H.; Chang, S.-H.; Wu, C.-G. Surface Engineering of ZnO Electron Transporting Layer via Al Doping for High Efficiency Planar Perovskite Solar Cells. *Nano Energy* **2016**, *28*, 311−318.

DOI: 10.1021/acsami.7b17798
ACS Appl. Mater. Interfaces 2018, 10, 835−844